Cracking the Code: LoRa Physical-Layer Insights and Signal Recovery under Cross-Technology Interference

Demin Gao, *Member, IEEE,* Ye Liu, *Senior Member, IEEE,* Qiaolin Ye, *Member, IEEE,* and Honggang Wang, *Fellow, IEEE.*

***Abstract*—Low-Power Wide-Area Networks (LPWANs) have emerged as a promising communication technology for the Internet of Things (IoT). However, frequency overlap among wireless networks using different radio technologies creates significant interference, compromising communication reliability. This challenge is particularly urgent in LoRa networks, which coexist in the 2.4 GHz ISM band with other IoT transmitters capable of transmitting at much higher power levels. In our study, we begin by providing a comprehensive understanding of the LoRa physical layer (PHY), including insights into modulation and demodulation mechanisms. Leveraging this knowledge, we successfully implemented a real-time LoRa PHY on the GNU Radio Software-Defined Radio platform. To address cross-technology interference during peak detection, we introduce a spectrum merging technique that maintains phase coherence between superimposed peaks, minimizing spectral leakage artifacts. Beyond that, our analysis actively enhances the performance of commercial LoRa devices. Furthermore, we systematically explore the interference dynamics between LoRa and IEEE 802.15.4g networks. Our rigorous investigation reveals LoRa's ability to achieve high packet reception rates, even in the presence of strong IEEE 802.15.4g interference.**

***Index Terms*—LoRa, Signal Recovery, Networks Coexistence, Cross Technology Interference**

I. Introduction

LOW-POWER Wide-Area Networks (LPWANs) [1] are designed for long-distance, low-data-rate communication, making them highly versatile for a wide range of applications within the Internet of Things (IoT) [2], [3]. Among the LPWAN technologies, LoRa (Long Range) [4] stands out as a prominent choice. LoRa excels in its communication capabilities, facilitating data transmission across tens of kilometers while maintaining minimal energy consumption and a low Signal-to-Noise Ratio (SNR) [5], [6]. Moreover, battery-powered LoRa nodes can remain operational for up to a decade, ensuring reliable and long-lasting connectivity [7]. Recently, Semtech has revolutionized the LoRa ecosystem with the introduction of the SX1280 LoRa chip [8]. Operating over the 2.4GHz spectrum [9], this chip offers extended long-range capabilities, a significant advancement in the field. In particular, LoRa is now a preferred solution in scenarios requiring low-latency connections or in remote locations where traditional networking solutions may be inaccessible [10], [11].

In the realm of extended-range transmissions and constrained transmission power, LoRa devices face significant interference challenges when operating in the 2.4 GHz spectrum [12]. The remarkable surge and ubiquitous embrace of the IoT in recent years have been truly extraordinary. A depiction of such a scenario, exemplified by a smart city. However, the wireless performance of such expansive networked systems can suffer greatly when less powerful IoT devices coexist with a multitude of wireless technologies, such as WiFi, ZigBee, and Bluetooth, all vying for access within the same spectrum [13]. This competition, particularly prevalent in the 2.4GHz ISM band, often results in cross-technology interference, leading to frequent transmission failures [14].

The research on LoRa cross-technology interference mitigation techniques has made significant progress. Frequency Hopping [15] is a common wireless communication interference mitigation technique that reduces long-term interference. Channel Bonding [16] increases data transmission rates by bonding multiple channels. Dynamic spectrum access [17] allows wireless devices to dynamically select the best communication channel based on the current spectrum usage. Despite the flexibility provided by DSA, it requires complex sensing mechanisms and rapid decision-making algorithms, which can be challenging in practical deployments. With the growth of IoT devices, LoRa networks deployed in dense environments face a variety of interference sources, including interference from different wireless technologies such as WiFi and ZigBee. These interference sources may overlap with LoRa signals in time and frequency, increasing the complexity of interference management.

The primary aim of this paper is not merely to mitigate interference from wireless traffic, but rather to bolster the coexistence of LoRa with other wireless networks that utilize overlapping frequency channels. In this paper, we present a new technique known as LoRaSR (LoRa Physical-Layer Signal Recovery), which is designed to reconstruct LoRa

Demin Gao is with the College of Information Science and Technology & Artificial Intelligence, Nanjing Forestry University, Nanjing 210037, China. (e-mail: dmgao@njfu.edu.cn).

Ye Liu (corresponding author) is with the College of Artificial Intelligence, Nanjing Agricultural University, Nanjing 210095, China (e-mail: yeliu@njau.edu.cn).

Qiaolin Ye is with the College of Information Science and Technology & Artificial Intelligence, the State Key Laboratory of Tree Genetics and Breeding, and the Co-Innovation Center for Sustainable Forestry in Southern China, Nanjing Forestry University, Nanjing 210037, China. (E-mail: yqlcom@njfu.edu.cn)

Honggang Wang is with the Department of Graduate Computer Science and Engineering, Katz School of Science and Health, Yeshiva University, New York, NY 10016 USA (e-mail: Honggang.wang@yu.edu).

signals. LoRaSR's primary objective is to mitigate interference among signal peaks and accurately recover peak characteristics, such as position and height, which may be distorted by Cross-Technology Interference (CTI). Our approach centers on identifying the chirp peak that aligns with each window, enabling the differentiation of peaks corresponding to different packets based on these synchronized chirps.

Our contributions are summarized as follows:

- We provide an extensive elucidation on the demodulation and decoding processes inherent to LoRa technology within academic discourse. Subsequently, we achieve a comprehensive real-time implementation of the LoRa physical layer using the GNU Radio Software-Defined Radio (SDR) platform.
- We are the pioneers in examining and quantifying interference patterns between LoRa and 802.15.4 networks at a bit-level granularity. We introduce a spectrum merging methodology where two peaks subjected to superposition maintain phase coherence, ensuring the mitigation of spectral leakage artifacts.
- The architectural conception of LoRaSR addresses the considerable challenge of decoding data embedded within LoRa chirps. Empirical results demonstrate the efficacy of LoRaSR in achieving signal recovery under cross-technology interference.

The remainder of this paper is organized as follows. Section II reviews related literature. Section III provides preliminaries. In Section IV, we delve into our insights on the LoRa physical layer. Next, we introduce the proposed LoRaSR in Section V. Performance evaluation results are discussed in Section VI. Lastly, Section VII provides a summary of our work.

II. Related Work

In this section, we review the related work of our work with respect to the following domains.

LoRa Sub-GHz and LoRa 2.4 GHz. LoRa, as the physical layer technology behind LoRaWAN, has garnered significant attention as one of the most successful low-power wide-area network solutions for the Internet of Things [18]–[20]. Research efforts [21]–[23] have explored its potential in diverse applications, such as industrial networks [24]–[26] and smart agriculture [10], [27], [28]. Comparative studies between LoRa sub-GHz and LoRa 2.4 GHz in both indoor and outdoor scenarios have been conducted [9], [29], shedding light on the challenges that need to be addressed to fully exploit this technology. Additionally, reverse engineering efforts have provided insights into the fundamental principles of LoRa's PHY layer [30].

LoRa Performance Enhancement. Efforts to enhance LoRa network capacity and throughput have led to the exploration of collision decoding and weak signal decoding. These approaches [31]–[33] leverage the unique characteristics of LoRa PHY demodulation to separate chirps and decode packets, thereby mitigating collision and interference issues [34]. Studies [35]–[37] have also examined the performance of LoRa in the presence of noise and interference, including the scalability challenges faced by LoRaWAN, and algorithms for mitigating interference among superposed LoRa signals [38].

Networks Coexistence. Coexistence studies have investigated the interaction between LoRa and other wireless technologies, such as ZigBee [39], [40] and Bluetooth [41], in the 2.4 GHz band. These studies explore message exchange protocols and assess the impact of interference on LoRa-based wireless links. Furthermore, investigations into cross-technology interference between LoRa and IEEE 802.15.4g networks have been conducted systematically [42]. Performance analyses of LoRa signals under interference from WiFi devices and adjacent channel interference from LTE systems have also been undertaken [12], [43]. Table. I provides a clear comparison of various studies on LoRa performance enhancement, network coexistence, and interference dynamics, highlighting the differences in objectives, methodologies, and outcomes.

In contrast to previous research, which primarily focused on avoiding channel interference, this paper delves into the specific characteristics of LoRa within the 2.4 GHz frequency bands and endeavors to recover LoRa signals under channel interference. To the best of our knowledge, this study represents the first exploration of LoRa signal recovery under interference. The proposed framework, LoRaSR, capitalizes on the physical properties of concurrent ZigBee/WiFi transmission to decode LoRa packets, enabling LoRa devices to establish connections with other LoRa devices. Thus, our investigation serves as both a complementary and orthogonal contribution to existing work in the field.

III. Preliminaries

A. Cross-Technology Interference Background

In LPWAN technologies such as LoRa, cross-technology interference is an increasingly severe issue. With the surge in IoT devices, the 2.4 GHz ISM band has become increasingly congested, with various wireless technologies such as WiFi, ZigBee, and Bluetooth all competing for limited spectrum resources. The frequency overlap among these technologies has led to significant interference issues, affecting the reliability of communication. Particularly in LoRa networks, since they coexist with other IoT transmitters in the same frequency band, and these transmitters may have much higher power levels, the interference challenges for LoRa devices in the 2.4 GHz band are particularly pronounced.

LoRa, as a LPWAN technology operating in the 2.4 GHz band, is susceptible to interference from other technologies operating in the same band. This interference not only affects the demodulation of signals but can also spoof LoRa devices. Therefore, signal recovery is crucial. To address this issue, we propose two solutions: a spectrum merging method to reduce spectral leakage artifacts and LoRa waveform reconstruction to enhance signal integrity.

B. The Role of the SDR Platform in Interference Management

The flexibility of the SDR platform plays a key role in managing and mitigating interference. The SDR platform can dynamically adjust signal processing algorithms, which is

This article has been accepted for publication in IEEE Transactions on Wireless Communications. This is the author's version which has not been fully edited and content may change prior to final publication. Citation information: DOI 10.1109/TWC.2025.3574576

TABLE I: Summary of Related Work on LoRa Performance Enhancement, Network Coexistence, and Cross-Technology Interference

Reference	Objective	Methods	Results	Novelty
Croce et al., 2020 [5]	LoRa link behavior and cell performance	Analysis of the LoRa PHY layer	Insights into link behavior and cell-level performance	Real-time LoRa PHY implementation
Gao et al., 2021 [12]	Coexistence of LoRa and WiFi	Detection of extremely LoRa weak signals	Enabled coexistence by detecting weak signals	Spectrum merging technique
Orfanidis et al., 2017 [42]	Interference between LoRa and IEEE 802.15.4g	Systematic investigation of interference dynamics	Revealed high packet reception rates despite interference	Focus on in-band interference
Gao et al., 2024 (This Work)	Real-time LoRa PHY and signal recovery under cross-technology interference	Implementation of LoRaSR (LoRa Signal Recovery)	Demonstrated efficacy of LoRaSR in achieving signal recovery	Real-time PHY and spectrum merging for robust signal recovery

crucial for dealing with variable interference scenarios. Moreover, the high data throughput and MIMO capabilities of the SDR platform are essential for advanced spectrum monitoring equipment to identify and mitigate interference sources. In our study, we leveraged the SDR platform to successfully implement the LoRa physical layer (PHY) and introduced a spectrum merging technique to address cross-technology interference during peak detection. This technique maintains phase coherence between superimposed peaks, minimizing spectral leakage artifacts.

Additionally, our analysis actively enhances the performance of commercial LoRa devices and systematically explores the interference dynamics between LoRa and IEEE 802.15.4g networks. The adaptability of the SDR platform enables it to address various interference scenarios, including multipath propagation, frequency-selective fading, and clutter echoes, which can cause signal distortions leading to errors in target detection and measurement. We discuss advanced signal processing techniques, such as adaptive filtering, digital beamforming, and interference cancellation algorithms, and detail their implementation on the SDR platform.

IV. LoRa PHY Insights

The LoRa modulation and demodulation schemes remain proprietary, with limited theoretical explication available. Existing patent documentation often lacks the necessary depth in mathematical equations and signal processing mechanisms. In this section, we aim to bridge this gap by providing a comprehensive understanding of the LoRa PHY, including detailed insights into its modulation and demodulation mechanisms.

A. Modulation

LoRa utilizes the Chirp Spread Spectrum (CSS) modulation mechanism [44], renowned for its exceptional long-range communication capability. This modulation technique operates on the principle of linear frequency modulation, where the chirp signal employed occupies a broad frequency band. Essentially, CSS modulation entails the continuous alteration of the transmitted signal's frequency over time, thus forming a chirp waveform. This waveform is generated by linearly sweeping the frequency of a carrier signal across a specified time duration. Consequently, the signal's frequency experiences a constant rate of increase or decrease, resulting in linear frequency modulation, as depicted in Fig. 1. Typically associated with low data rates, CSS modulation ensures a longer chirp period, enabling the signal to sustain an elongated

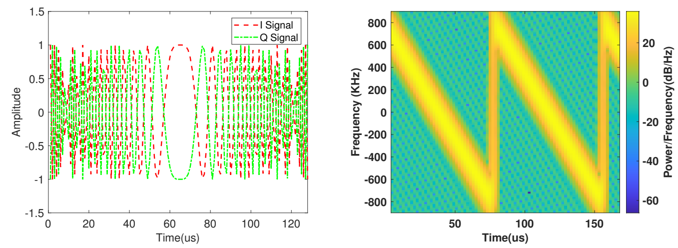

(a) LoRa signal time domain (b) LoRa signal frequency domain

Fig. 1: Chirp Spread Spectrum modulation involves the modulation of a signal's frequency, wherein the frequency either increases or decreases at a constant rate.

transmitted waveform. This prolonged chirp duration enhances the signal's energy and augments its propagation capability over extended distances.

Distinct symbols are distinguished by manipulating the initial frequency in different chirp signals. The relationship between the starting frequency f_0 and the symbol value M can be expressed as:

$$f_0 = \frac{M}{2^{SF}} \times BW \tag{1}$$

where, BW represents the channel bandwidth and SF represents the Spreading Factor (typically taking values from the set $\{7, 8, 9, 10, 11, 12\}$). Throughout the entire modulation symbol period, the baseband frequency $f_B(t)$ can be represented as follows:

$$f_B(t) = \begin{cases} f_0 - \frac{BW}{2} + kt & ,0 \leq t \leq t_1 \\ k(t-t_1) - \frac{BW}{2} & ,t_1 \leq t \leq T_{sym} \end{cases} \tag{2}$$

where, $t1 = (2^{SF} - M)/BW$, $T_{sym} = 2^{SF}/BW$, $k = BW^2/2^{SF}$. Once the signed frequency sweep signal $f_B(t)$ is obtained, the subsequent step involves generating a sinusoidal signal with a frequency adjusted to meet specific criteria. Given the fulfillment of the integral relationship between phase and frequency, the associated phase value of the signal $\varphi_B(t)$ is expressed as follows:

$$\varphi_B(t) = \begin{cases} f_0 t - \frac{BW}{2} t + \frac{1}{2} k t^2 \\ \frac{1}{2} k (t-t_1)^2 - \frac{BW}{2}(t-t_1) + \psi(t_1) \end{cases} \tag{3}$$

The phase at the end of the initial modulation segment, denoted by $\psi(t_1)$, serves as the starting phase for the subsequent

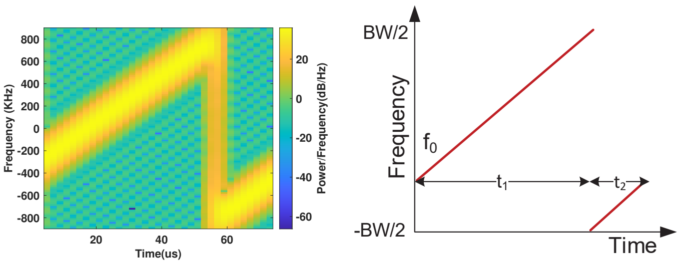

(a) CSS baseband (b) Two up-chirp signal

Fig. 2: The implementation of CSS baseband for LoRa involves transmitting a numerical value.

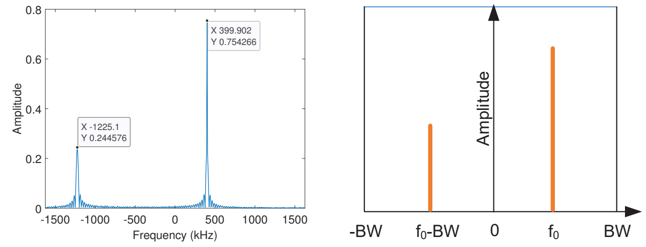

(a) Frequency domain for bit '63' (b) Two spectral peak for '63'

Fig. 3: When the symbol value is 63, the signal spectrum within the bandwidth BW.

modulation segment to ensure signal phase continuity. The fundamental principle underlying LoRa CSS demodulation involves extracting the initial frequency of the signal after removing a portion of the linear frequency sweep component, thereby obtaining the corresponding code value, as shown in Fig. 2. One conventional approach for LoRa CSS demodulation involves multiplying the captured sampling signal by the standard down-chirp signal to eliminate the linear sweep signal. Subsequently, an FFT operation is applied to the processed signal to identify the code, allowing for the determination of the current symbol value based on its frequency. Therefore, the frequency expression of the signal can be represented mathematically as follows:

$$f_D(t) = \frac{BW}{2} - kt, 0 \leq t \leq T_{sym} \tag{4}$$

Assuming an initial phase of 0, the CSS modulation signal and the down-chirp signal corresponding to symbol value M can be represented as follows:

$$\begin{aligned} S_M(t) &= e^{j2\pi\varphi_B(t)}, 0 \leq t \leq T_{sym} \\ S_D(t) &= e^{j2\pi\varphi_D(t)}, 0 \leq t \leq T_{sym} \end{aligned} \tag{5}$$

B. Demodulation

After signal reception, the LoRa device necessitates signal demodulation, a process that involves executing a multiplication operation between the received signal and the down-chirp signal. This critical step enables the extraction of the transmitted information from the modulated waveform, facilitating effective communication across the intended frequency spectrum. We have observed that this method not only enhances the signal fidelity but also optimizes the device's performance in diverse environmental conditions. We have,

$$s_{de}(t) = S_M(t) \times S_D(t) \tag{6}$$

Since $S_M(t)$ is expressed as a piecewise function, each segment of the piecewise function is delineated separately. Assuming the symbol to be transmitted is denoted as S, the baseband signal undergoes a frequency scan in the following manner: in the first segment, the frequency is swept from $f_0 - BW/2$ to $BW/2$, while in the second segment, the frequency is swept from $-BW/2$ to f_0. This completes the CSS modulation's frequency linear scan across the entire symbol duration. For the interval $0 \leq t \leq t_1$, based on Equation (5) and Equation (3), the signal to be demodulated is as follows:

$$S_{M1}(t) = e^{j2\pi((f_0 - \frac{1}{2}BW)t - \frac{1}{2}kt^2} \tag{7}$$

According to the previous analysis, demodulating the $S_{M1}(t)$ signal, it is multiplied with the down-chirp signal. In $0 \leq t \leq t_1$, according to Equation (7) and Equation (5), the result $S_{M1}(t)S_{D1}(t)$ is,

$$S_{M1}(t) \times S_{D1}(t) = e^{j2\pi f_0 t} \tag{8}$$

From Equation (8), it is apparent that during the initial time period, after the modulation signal undergoes multiplication by the standard down-chirp signal, the influence of frequency linear sweep is eliminated, leading to the ideal generation of a sinusoidal signal with the frequency f_0. Now, let us examine the signal demodulation in the interval $t_1 \leq t \leq T_{sym}$.

$$S_{M2}(t) \times S_{D2}(t) = e^{j2\pi((f_0 - BW)t + \varphi_{M1}(t_1) + \varphi_{D1}(t_1))} \tag{9}$$

In Equation (9), the modulation signal undergoes multiplication by the standard down-chirp signal during the second time period, effectively canceling out the frequency linear sweep. This ideally yields a sinusoidal signal with a frequency of $f_0 - BW$. Consequently, when the LoRa CSS-modulated waveform is multiplied by the standard down-chirp signal, it produces the output waveform and signal frequency. Due to the limited transmission bandwidth in LoRa communication, different symbols have distinct starting frequency sweep signals. This allows for the completion of the linear sweep across the entire bandwidth throughout the symbol transmission duration.

Note that, when the symbol falls within the range of 0 to $2^{SF-1} - 1$, the amplitude of the signal after FFT in the frequency band of $0 \sim BW$ is greater. Conversely, when the symbol falls within the range of 2^{SF-1} to $2^{SF} - 1$, the amplitude of the signal in the frequency band of $-BW \sim 0$ is larger after FFT. The analysis of Fig. 3 suggests that obtaining the initial frequency of the LoRa signal within the range of $0 \sim BW$ is sufficient for accurately computing the transmitted data. This is crucial for practical LoRa-based communication systems, indicating that precise estimation of the initial frequency facilitates successful data retrieval without exhaustive frequency measurements across the entire bandwidth.

V. LoRa Signal Recovery under Cross-Technology Interference

Building upon these characteristics, we propose a new signal recovery approach designed to mitigate the effects of cross-technology interference in this section.

A. Theoretical Analysis of Cross-Technology Interference

Interference can often be described using mathematical models where signal superposition, attenuation, and noise levels are key parameters. In the case of LoRa, due to its use of spread spectrum technology, the signal propagates over a wider frequency range, making it more susceptible to interference from other technologies. As signals propagate, they encounter various obstacles and environmental factors that cause signal attenuation. The long-distance propagation characteristic of LoRa signals makes them particularly vulnerable to multipath effects and obstruction by buildings in urban environments.

The design of LoRa signals takes into account the needs for long-distance transmission and low power consumption, but their performance may be affected in high-interference environments. The LoRa signal requires precise demodulation at the receiver, and any distortion caused by interference can lead to demodulation failure. Interference signals may overlay parts of the LoRa signal, preventing the receiver from correctly identifying the signal's initial frequency, thus failing to demodulate correctly. Additionally, interference can introduce additional noise, reducing the signal-to-noise ratio of the signal and further affecting signal demodulation.

B. Cross-Technology Interference for LoRa

The transmission process involves emitting a wireless signal from the transmitter, which undergoes attenuation over distance before reaching the receiver. Upon reception, the signal appears distorted, often overlaid with other wireless signals nearby. Subsequently, the signal undergoes decoding, treating the collective ongoing signal transmissions as noise. The success of decoding is a stochastic event, dependent on factors such as desired signal strength, thermal noise levels, and the intensity of interfering signals. The broadcast nature of the wireless medium makes it inherently susceptible to interference from spatially proximate concurrent transmissions that overlap in both time and frequency.

This challenge is particularly accentuated in the ISM bands, where the number and diversity of coexisting wireless networks continue to grow. Traditional coexistence strategies primarily attempt to address interference by employing carrier sense (a basic access mechanism that attentively accommodates other transmitters) or transmission across orthogonal channels. However, these approaches may make low-power technologies more vulnerable to starvation or may become impractical due to the limited availability of interference-free channels, respectively. Our focus is on investigating cross-technology interference. Specifically, we are examining scenarios of in-band interferences, with particular attention directed toward adjacent coexistence, as depicted in Fig. 4.

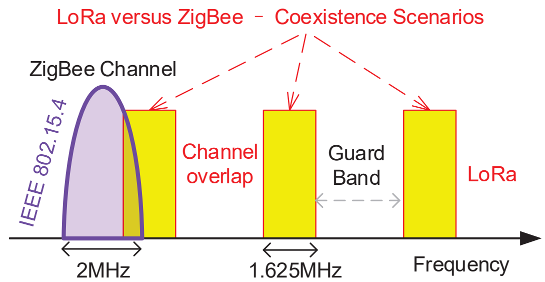

Fig. 4: Coexistence scenarios between LoRa and ZigBee in the 2.4 GHz ISM band.

It is worth noting that Physical-layer Cross-Technology Communication (PHY-CTC) [45] enables seamless data exchange among diverse IoT devices, even with different technologies. If a ZigBee device's waveforms resemble those of a LoRa transmitter, LoRa receivers can decode the signals accurately. However, cross-technology interference not only disrupts LoRa signal demodulation but can also spoof LoRa devices. Signal recovery is vital. To address this, we propose two solutions: a spectrum merging methodology to reduce spectral leakage artifacts and LoRa waveform reconstruction to enhance signal integrity.

C. Spectrum Merging for Mitigating Spectral Leakage

We analyze the impact of interference on the transmitted data signal during the time interval t_2, as depicted in Fig. 5. Fig. 5a illustrates a temporal graph showing the evolution of a signal over time. The linearly increasing frequency function $f(t)$ is derived from a linear frequency sweep applied to a signal with a bandwidth of 1625 kHz, spreading factor of 6, and sampling rate of 20. This signal is achieved through baseband modulation of $f(t)$. Fig. 5b presents a temporal-noise profile, showing the absence of noise interference in the interval 0-39.5 μs., with noise interference of 3.5 dB intensity occurring in the interval 30-39.5 μs.

A spectral diagram is depicted in Fig. 5c. Typically, the post-demodulation spectrum of the LoRa signal should display a dual-peak pattern. However, the graph shows three distinct peaks. In the temporal segment labeled as $t1$ (0-39.5μs), the signal remains unaffected, while during $t2$ (30-39.5μs), noise disturbance occurs (e.g., from a ZigBee signal, as shown in Fig. 2b). Leveraging the robust anti-interference capabilities inherent in LoRa modulation, if the noise peak remains lower than the signal peak, indicating the noise's inability to overpower the signal, the receiver can still demodulate the data by distinguishing between the signal and the noise. Thus, successful signal demodulation is achieved.

Illustrated in Fig. 3a (Section IV-B), a segment of the payload chirp containing frequencies exceeding half of the bandwidth $(BW/2)$ undergoes a realignment, causing them to be down-shifted to the lowest frequency at $-BW/2$. This realignment results in the emergence of two distinct frequencies within the chirp output. To address energy loss during peak detection, we design a Spectrum Merging Methodology (SMM). This method involves transforming the spectrum spanning $(-BW, 0)$ by shifting the FFT output from the

This article has been accepted for publication in IEEE Transactions on Wireless Communications. This is the author's version which has not been fully edited and content may change prior to final publication. Citation information: DOI 10.1109/TWC.2025.3574576

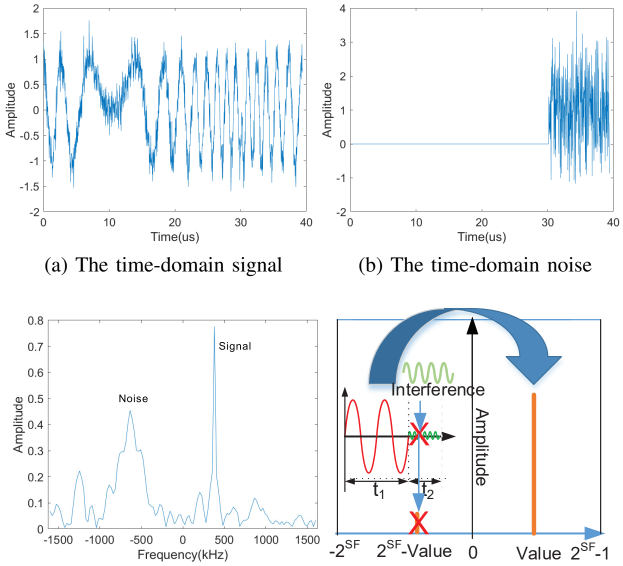

(a) The time-domain signal (b) The time-domain noise

(c) Signal and noise overlapping (d) signal interference in t_2

Fig. 5: Despite experiencing interference during the t_2 time period, the data decoding remains resilient and impervious to adverse effects.

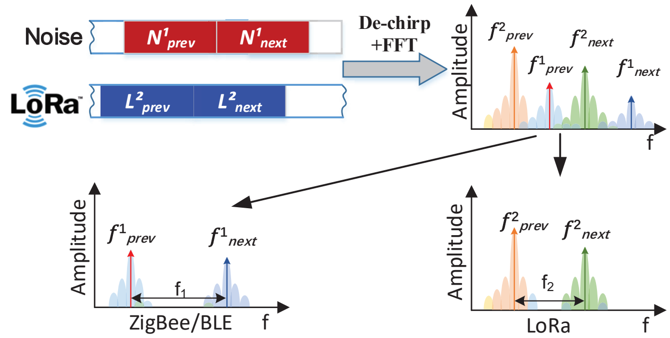

Fig. 6: Standard LoRa decoding amidst collisions generates multiple frequency peaks, leading to confusion. LoRaSR eliminates these interfering frequency peaks.

negative frequency domain to the positive frequency domain $(0, BW)$. As a result, the peak initially located at $f_0 - BW$ in the original spectrum now occupies the frequency f_0 (as defined in Equation 8). Integrating the inverted spectrum with the original one facilitates the accumulation of energy from both FFT peaks. For this merging to be effective, it is crucial that the two peaks subjected to superposition maintain phase coherence, ensuring the mitigation of spectral leakage artifacts.

The analysis demonstrates that despite interference during this temporal interval, the data decoding process remains robust and unaffected, thanks to the SMM. This highlights the inherent resilience of the LoRa communication framework against interference, making it suitable for various practical scenarios and demanding operational contexts. These findings are particularly significant for applications relying on LoRa technology, especially in environments where interference or signal fluctuations are common due to environmental factors or concurrent wireless systems. Therefore, the proven durability of the data decoding mechanism against temporal interference enhances the appeal and reliability of LoRa technology in modern communication systems.

D. LoRa Signal Recovery through Waveform Reconstruction

The primary objective of waveform reconstruction is to recover the LoRa waveform lost due to cross-technology interference. The parameters SF and BW collectively determine the angle θ formed by the LoRa waveform and the abscissa ($\theta = \frac{(BW)^2}{2^{SF}}$). Hence, having access to a segment of the LoRa waveform enables the theoretical reconstruction of the entire waveform. We achieve waveform reconstruction by carefully analyzing decoded bits, which are readily available in software, ensuring compatibility with off-the-shelf LoRa hardware.

Initially, coded bits undergo a transformation into decoded bits. However, heightened interference from cross-technology signals compromises the efficacy of the channel decoder, resulting in decoded bits that are not an accurate representation of the coded bits. The coded bits are then mapped onto the frequency domain, with each discrete LoRa signal occupying a narrowband. LoRaSR employs fast Fourier transform (FFT) as a pivotal step in waveform reconstruction. This transformative operation enables LoRaSR to intricately reconstruct the original information encoded within the transmitted signals.

All waveforms, including LoRa, ZigBee, BLE, and noise, are multiplied with a standard down-chirp signal and subjected to fast Fourier transform (FFT). Following the de-chirp FFT process, each signal generates distinct peaks at different frequencies at the LoRa receiver. LoRaSR exploits signal characteristics between ZigBee/BLE and LoRa, allowing it to discern and isolate these signals. ZigBee/BLE and LoRa frequencies differ, with ZigBee waveforms typically occupying frequencies of $\pm$500kHz due to a signal tone period of $2\mu s$. Assuming an FFT time window of $80\mu s$, the frequency resolution of the FFT is $f_{res} = 1/80\mu s = 12.5$kHz. Consequently, the locations of ZigBee peaks can be calculated as $f_1 = \pm 500/12.5 = \pm 40$. Fig. 6 illustrates the scenario where ZigBee and LoRa peaks can be distinguished.

For a LoRa symbol, the number of possible peak locations depends on the symbol cardinality, which defines the size of the symbol set. For instance, if a LoRa symbol corresponds to two bits, there will be four possible peak locations: the 0^{th}, 32^{th}, 64^{th}, and 96^{th} FFT bins when the FFT size is set to 128. The frequencies of BLE waveforms typically range within $\pm$250kHz due to a frequency deviation of 250kHz in GFSK modulation. Therefore, the locations of BLE peaks are calculated as $f_1 = \pm 250/12.5 = \pm 20$. In this scenario, ZigBee/BLE peaks will not overlap with LoRa peaks, making them easily distinguishable.

VI. Evaluation

In this section, we conduct comprehensive experiments to assess the performance of LoRaSR across different scenarios.

This article has been accepted for publication in IEEE Transactions on Wireless Communications. This is the author's version which has not been fully edited and content may change prior to final publication. Citation information: DOI 10.1109/TWC.2025.3574576

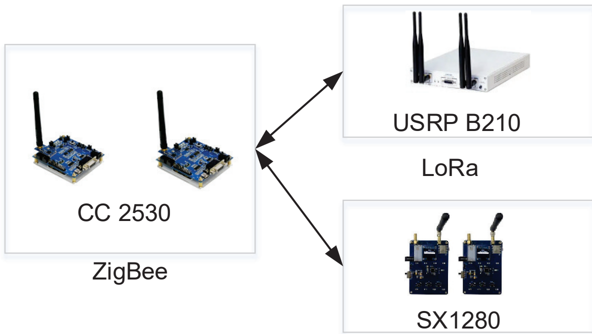

Fig. 7: Experimental Testbed of LoRaSR.

A. Hardware

Fig. 7 illustrates the experimental setup of the LoRaSR system. In our experiment, Additive Gaussian White Noise (AWGN) [46] and ZigBee serve as interference signal sources to disrupt the LoRa signal. While we use ZigBee as an example in this paper, the methodology is applicable to other interference scenarios as well. Other communication technologies such as WiFi and Bluetooth can also be utilized as interference sources with similar effects. The LoRaSR system is implemented using USRP-B210 platform with LoRa PHY. The sender (i.e., ZigBee) operates on commercial chips, specifically the Atmel AT86RF233 compliant with the IEEE 802.15.4g standard, with a default transmission power of 0dBm. The LoRaSR receiver (i.e., LoRa receiver, Semtech SX1280 chip) employs a bandwidth of 1.625MHz and a spreading factor of 8, with the channel frequency set at 2.4 GHz. Table. II summarizes the key parameters that were utilized in the simulations and experiments described within the document.

TABLE II: Simulation Parameters Summary

Parameter	**Value/Description**
Bandwidth	1.625 MHz
Spreading Factor	7, 8, 9, 10, 11, 12
Channel Frequency	2.4 GHz
Transmission Power	0 dBm (for ZigBee transmitter)
Signal Strength	30 dBm (for LoRa signal in tests)
Noise	AWGN, SNR of 10 for some tests
Sampling Rate	20 (assumed from context)
FFT Size	128

The GNU Radio framework serves as the core software for our SDR platform. GNU Radio is an open-source toolkit that provides a wide array of signal processing blocks and allows for the rapid development of SDR applications.We utilized Python as the primary programming language for developing the LoRa physical layer and other custom signal processing modules due to its versatility and the robust support it offers for integrating with GNU Radio. The LoRa physical layer was implemented by developing custom modules in GNU Radio that emulate the modulation and demodulation processes specific to LoRa. These modules include the CSS modulator and demodulator, which are essential for generating and recovering LoRa signals. The CSS modulator linearly sweeps the frequency of the transmitted signal, while the demodulator performs the inverse operation to retrieve the original data.

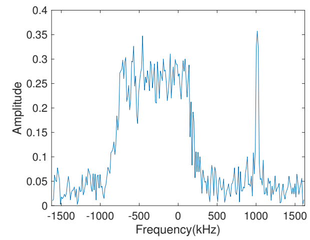

(a) The spectrum under interference 30-79 μs

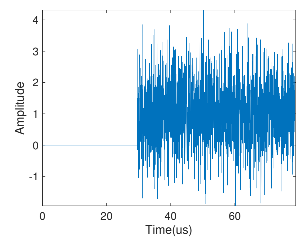

(b) The noise time with 30-79 μs

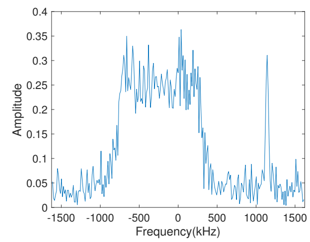

(c) The spectrum under interference 20-79 μs

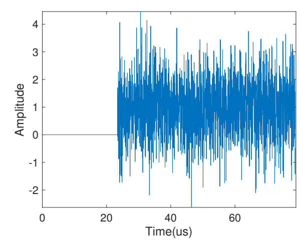

(d) The noise time with 20-79 μs

Fig. 8: The LoRa signal experiences time-domain interference from Additive White Gaussian Noise (AWGN) with increasing noise duration, while maintaining a constant amplitude of 4 dB.

B. LoRa Signal under Cross-Technology Interference

Fig. 8 illustrates the interference of the LoRa signal in the time domain by AWGN. Fig. 8b depicts a time-noise plot, showcasing interference caused by a 4dB noise during the t_2 period ($30\mu s \sim 79\mu s$) of the signal when the transmission symbol value is set to 80. Meanwhile, Fig. 8a presents a spectrum diagram. During the t_1 period ($0 \sim 30\mu s$), the signal remains undisturbed by interference, while during t_2, it encounters 4dB noise. Since the noise peak is lower than the signal peak during this period, the receiver can utilize the signal-noise difference for demodulation, enabling successful signal recovery. The time-noise plot in the figure delineates the interference period ($20\mu s \sim 79\mu s$) with 4 dB noise when the transmission symbol value is 90.

From Fig. 8c, during the t_1 period, the signal remains undisturbed by interference, whereas during t_2, it encounters 4dB noise. Since the noise peak surpasses the signal peak during this period, the receiver cannot differentiate the data from the noise, leading to unsuccessful demodulation. These experiments demonstrate that as the symbol value increases, the duration of noise interference during t_2 also increases. Consequently, the signal weakens progressively, eventually succumbing to noise dominance, rendering it undecodable.

Fig. 9 illustrates changes in signal and noise intensities following reception and modulation by the receiver. This change coincides with an increase in noise interference amplitude while maintaining a constant duration. Despite this, the

This article has been accepted for publication in IEEE Transactions on Wireless Communications. This is the author's version which has not been fully edited and content may change prior to final publication. Citation information: DOI 10.1109/TWC.2025.3574576

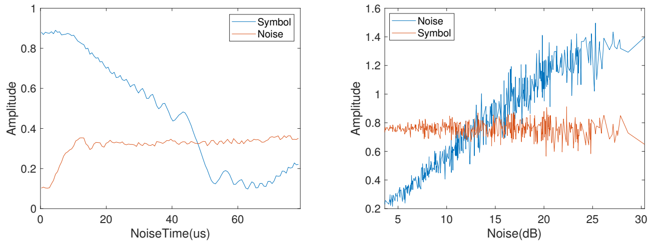

(a) Interference varies time (b) Interference varies signal strength

Fig. 9: The signal and noise intensities following reception and modulation by the receiver.

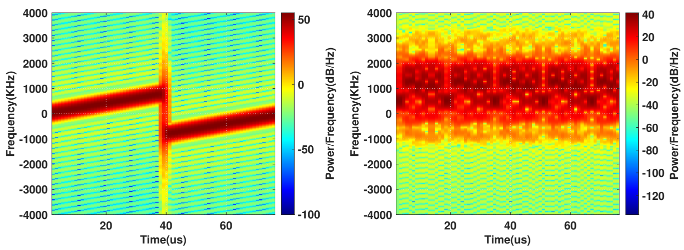

(a) LoRa signal (b) ZigBee signal

Fig. 10: The time spectrum diagram illustrating both the LoRa and ZigBee signals generated during the simulation.

signal intensity remains relatively stable, displaying a consistent trend upwards. Fig. 9b demonstrates a scenario where noise intensity remains constant, while an extension of noise interference duration leads to noticeable fluctuations in both signal and noise intensities post-reception and modulation.

In this context, a notable observation arises: the prolongation of noise interference duration leads to a decline in signal strength. Particularly, from 0 to 10 μs, the signal strength gradually diminishes due to increasing noise interference, resulting in amplified noise intensity. Subsequently, spanning 10 to 79 μs, noise intensity exhibits minimal variation, indicative of LoRa's inherent anti-interference properties. At this juncture, once noise intensity reaches a threshold, it stabilizes, reflecting LoRa's resilience against interference.

C. LoRa Signal Experiencing Interference from ZigBee Signal

We utilized the ZigBee signal as an interference source to examine the demodulation process of individual LoRa symbols. To elucidate the interference impact on LoRa demodulation, we conducted symbol-level modulation and demodulation simulations. The simulated environment featured LoRa parameters: BW = 1625 kHz, SF = 7, and a central frequency of 0 Hz, with a signal strength set to 30 dBm. Gaussian white noise with an SNR of 10 was introduced to emulate real-world conditions. The experimental setup is illustrated in Fig. 10.

To initiate our investigation, we introduced interference into the LoRa signal using a ZigBee signal with a power of 30 dBm, as depicted in Fig. 11. Sub-figures (e-h) within Fig. 11 displayed the resulting frequency domain characteristics after multiplying the LoRa signal by the descending edge signal. Simultaneously, sub-figures (a-d) within the same figure illustrated the extent of frequency domain coverage of the interfered LoRa signal, ranging from 0% to 100%. Upon examination of sub-figures (e-h) in Fig.11, it became evident that despite varying degrees of interference coverage, the demodulation process exhibited minimal discernible impact. The transmitted LoRa symbol could still be readily identified by locating the highest column.

We next examined the demodulation process when the latter half of a LoRa symbol was subjected to ZigBee signal interference. In Fig. 12, ZigBee signals with power levels ranging from 5 dBm to 45 dBm were introduced to interfere with the latter half of the LoRa symbol. When the ZigBee power was set to 5 dBm, as shown in (a, e) in Fig. 12, the low ZigBee power had minimal impact on the LoRa signal. However, with a ZigBee power of 45 dBm, multiple prominent peaks emerged, as seen in (h), resulting in failed LoRa demodulation.

Fig. 14 plots the LoRa signal experiences disruption due to interference from ZigBee signals. The power of the LoRa signal generated by the emulation is 30 dBm, and Gaussian white noise with an SNR of 10 is added to it. we will use simulated ZigBee signals to interfere with the LoRa signal. As shown in Fig 14a, we gradually increase the frequency domain of the interference signal ZigBee until the LoRa signal appears in the time domain as half a symbol after interference. In Fig 14b, it can be observed that right peak keeps in the frequency domain, and the LoRa signal can be also demodulated successfully.

D. Frame Reception Rate

In our study, we evaluated LoRa frame reception ratios (FRR) in two distinct environments: a laboratory within a building and an outdoor scenario. PRR is a critical metric in wireless communication networks, as it directly indicates the reliability of the network to deliver packets successfully. It was selected to evaluate how effectively our proposed solutions maintain communication reliability in the presence of interference. With LoRa's spectrum overlapping ZigBee's by 1/5, interference from ZigBee signals affected a portion of the frequency band. Fig. 15 illustrates the average FRR of LoRa frames across varying distances.

Despite a gradual decrease in FRR in noisy indoor environments, with rates dropping to around 95% between distances of 100 to 500 meters, LoRaSR showcased a remarkable FRR of over 93% even at a distance of 500 meters in corridor settings. Across different locations and distances, LoRaSR consistently achieved FRRs of 98% or higher, demonstrating its ability to reliably collect data from various LoRa devices and its compatibility with heterogeneous LoRa systems. These results highlight LoRa's resilience in data decoding despite interference.

E. Symbol Error Ratios

Fig. 16 illustrates the Symbol Error Rate (SER) of LoRaSR under various experimental setups, particularly scenarios where the LoRa spectrum partially overlaps with the ZigBee

This article has been accepted for publication in IEEE Transactions on Wireless Communications. This is the author's version which has not been fully edited and content may change prior to final publication. Citation information: DOI 10.1109/TWC.2025.3574576

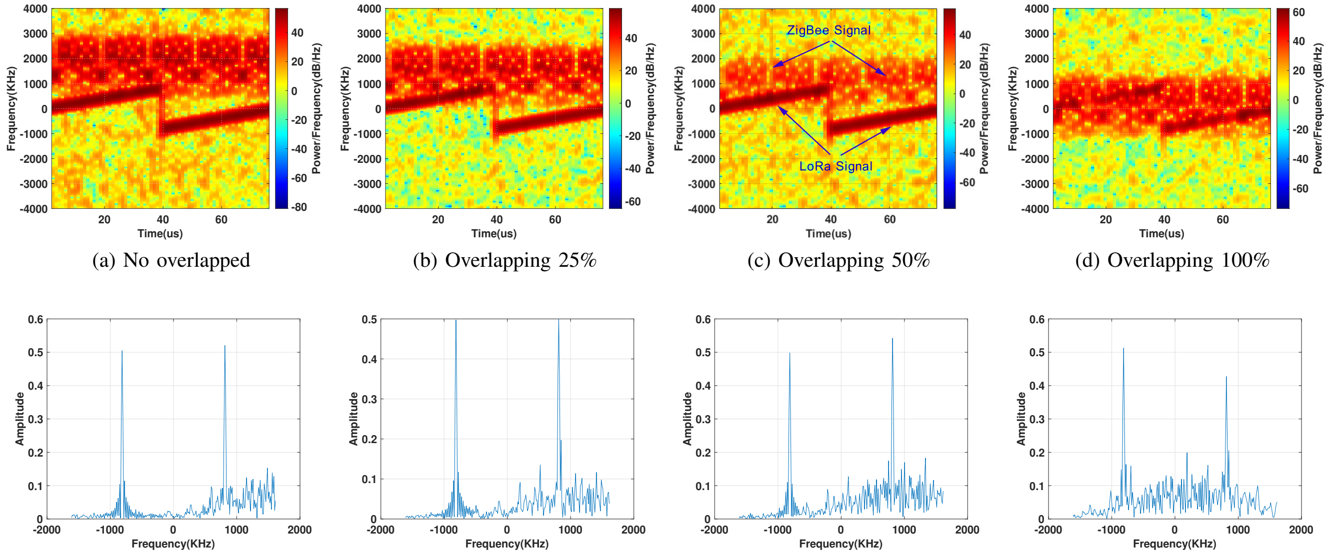

(a) No overlapped (b) Overlapping 25% (c) Overlapping 50% (d) Overlapping 100%

(e) LoRa decoding Fig. 11a (f) LoRa decoding Fig. 11b (g) LoRa decoding Fig. 11c (h) LoRa decoding Fig. 11d

Fig. 11: The LoRa signal is interfered by ZigBee signal with different overlapped bandwidth

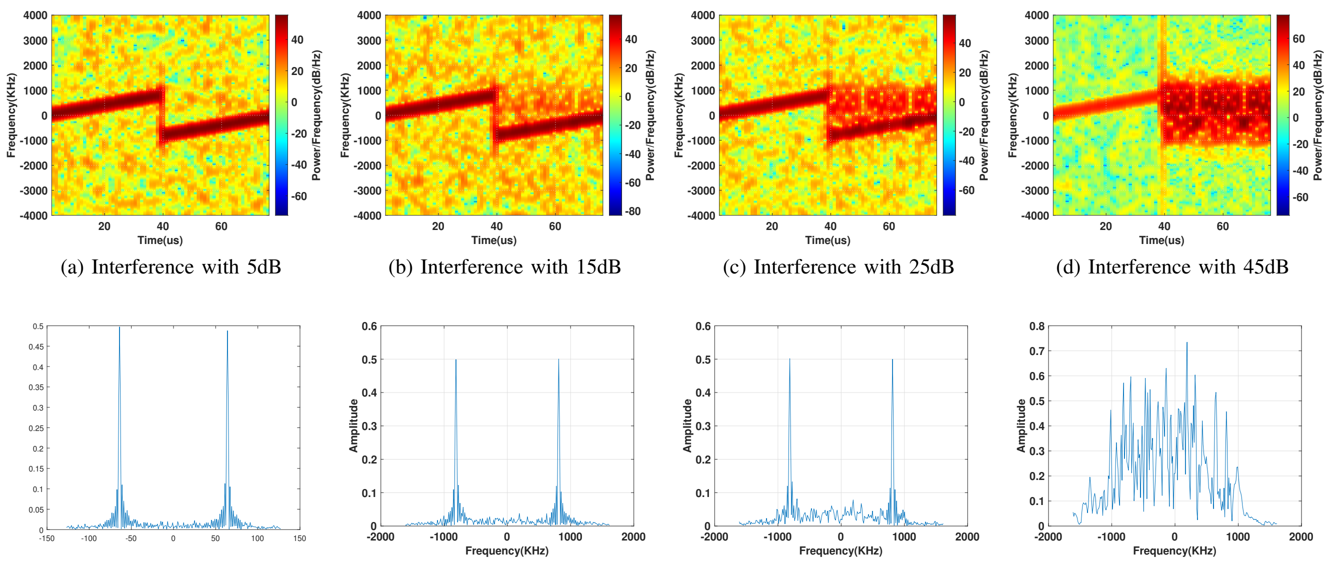

(a) Interference with 5dB (b) Interference with 15dB (c) Interference with 25dB (d) Interference with 45dB

(e) LoRa decoding Fig. 12a (f) LoRa decoding Fig. 12b (g) LoRa decoding Fig. 12c (h) LoRa decoding Fig. 12d

Fig. 12: The interference of the LoRa signal by the ZigBee signal occurs during the time period $t2$, with varying ZigBee signal strengths.

spectrum by fractions of 1/5 and 2/5. SER provides insight into the bit-level accuracy of the demodulation process. By assessing the SER, we can understand the precision with which our signal recovery techniques can reconstruct the transmitted symbols despite interference. Notably, LoRaSR consistently demonstrates exceptional performance, maintaining a low error ratio consistently below 0.3%, particularly evident within a 250-meter range. These findings emphasize the resilience and reliability of LoRa signals, especially when configured with narrower bandwidths, owing to their prolonged symbol duration. However, challenges arise with increased distance, leading to a noticeable decline in performance, highlighting the complexities of accurately reconstructing LoRa signals over extended distances.

F. In-Depth Analysis of Experimental Results

The experimental data revealed that in interference-free or low-interference environments, the Packet Reception Rate (PRR) of LoRa signals was very high, indicating the excellent communication performance of LoRa technology under ideal conditions. However, as the strength of the interference signal increased, particularly when the power of the interference signal approached or exceeded that of the LoRa signal, the PRR began to decline significantly. This trend aligns with our expectations and is consistent with existing literature,

This article has been accepted for publication in IEEE Transactions on Wireless Communications. This is the author's version which has not been fully edited and content may change prior to final publication. Citation information: DOI 10.1109/TWC.2025.3574576

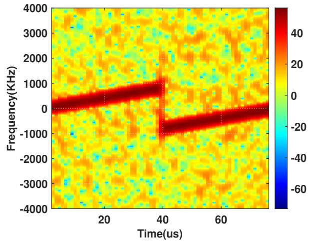

(a) Interference with 5dB

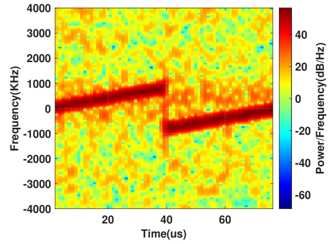

(b) Interference with 15dB

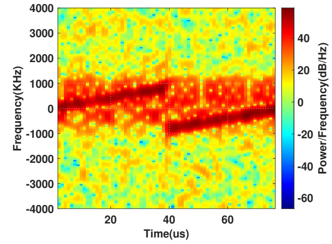

(c) Interference with 25dB

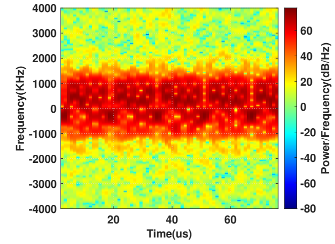

(d) Interference with 45dB

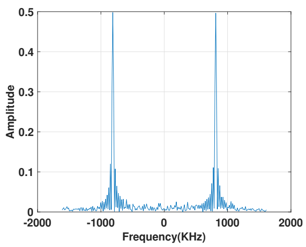

(e) LoRa decoding Fig. 13a

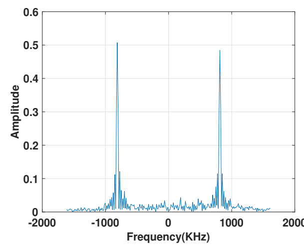

(f) LoRa decoding Fig. 13b

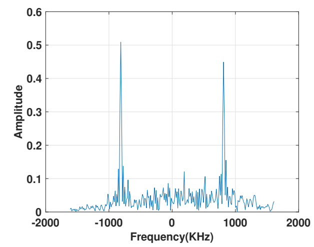

(g) LoRa decoding Fig. 13c

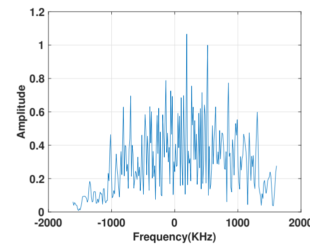

(h) LoRa decoding Fig. 13d

Fig. 13: The LoRa signal experiences interference from ZigBee signals of varying strengths, causing absolute overlap of the LoRa spectrum with the ZigBee signal.

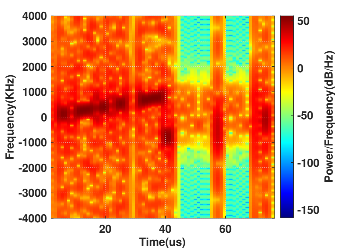

(a) LoRa signal

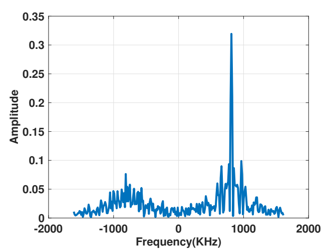

(b) LoRa decoding

Fig. 14: The LoRa signal experiences disruption due to interference from ZigBee signals.

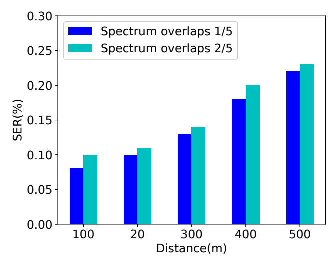

(a) SER (Building scenario)

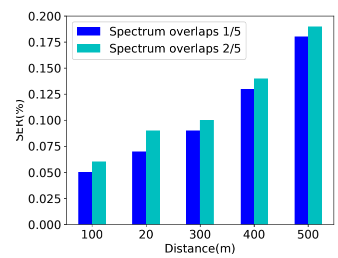

(b) SER (Outdoor scenario)

Fig. 16: Performance of LoRa (Spreading Factor = 8).

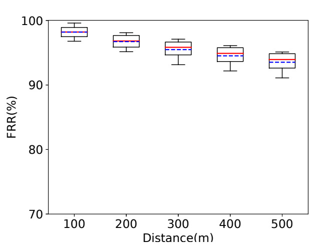

(a) FRR (Building scenario)

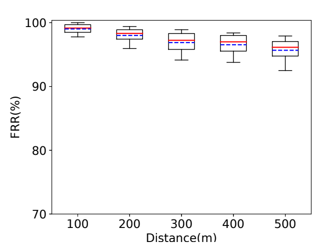

(b) FRR (Outdoor scenario)

Fig. 15: Frame Reception Ratios in the presence of LoRa-ZigBee spectrum overlap by 1/5.

which suggests that the robustness of LoRa signals in high-interference environments is limited.

The experimental results were largely consistent with the predictions of theoretical models. At low Signal-to-Noise Ratios (SNR), the demodulation process of LoRa signals could accurately recover the signals, which is in line with the anti-interference capabilities of LoRa's CSS modulation mechanism. However, at high SNR, due to the peak of the interference signal potentially exceeding the peak of the LoRa signal, the demodulation process failed. This phenomenon is in aligns with theoretical analysis, further validating the effectiveness of our experimental design and execution.

VII. Conclusion

In this study, we conducted experiments to investigate LoRa cross-technology interference under various conditions and thoroughly analyzed the obtained results. Our research entailed a comprehensive examination of LoRa characteristics. Through empirical investigations, we identified incorrect symbols, enabling the proposed LoRaSR to reconstruct complete LoRa frames. Using a prototype implementation of LoRaSR with the USRP B210 platform and standard LoRa chips, we demonstrated the feasibility of this approach. In addition, our study identified certain areas for allocating channels to ensure reliable and efficient communication, particularly regarding channel allocation in adjacent areas. To address these shortcomings, we conducted extensive experiments to evaluate LoRaSR's performance. The results affirm its ability to reliably transmit LoRa communication even in the presence of cross-technology interference. Moreover, our findings suggest that the proposed method holds significant promise for grazing applications. We believe it offers a valuable perspective for mitigating interference issues in LoRa across various scenarios.

ACKNOWLEDGMENT

This work was supported by National Nature Science Foundation of China No. 32371877, the Future Network Scientific Research Fund Project (Grant No. FNSRFP-2021-YB-17) and The Priority Academic Program Development(PAPD) of Jiangsu Higher Education Institutions.

REFERENCES

[1] C. Milarokostas, D. Tsolkas, N. Passas, and L. Merakos, "A Comprehensive Study on LPWANs With a Focus on the Potential of LoRa/LoRaWAN Systems," *IEEE Communications Surveys & Tutorials*, vol. 25, no. 1, pp. 825–867, 2023.

[2] T. Janssen, A. Koppert, R. Berkvens, and M. Weyn, "A Survey on IoT Positioning Leveraging LPWAN, GNSS, and LEO-PNT," *IEEE Internet of Things Journal*, vol. 10, no. 13, pp. 11 135–11 159, 2023.

[3] W. Jiao, T. Tang, W. Zhou, "Delay-sensitive energy-efficient routing scheme for the Wireless Sensor Network with path-constrained mobile sink, " *Ad Hoc Networks*, 158: 1-17, 2024.

[4] M. Jouhari, N. Saeed, M.-S. Alouini, and E. M. Amhoud, "A Survey on Scalable LoRaWAN for Massive IoT: Recent Advances, Potentials, and Challenges," *IEEE Communications Surveys & Tutorials*, vol. 25, no. 3, pp. 1841–1876, 2023.

[5] D. Croce, M. Gucciardo, S. Mangione, G. Santaromita, and I. Tinnirello, "LoRa Technology Demystified: From Link Behavior to Cell-Level Performance," *IEEE Transactions on Wireless Communications*, vol. 19, no. 2, pp. 822–834, 2020.

[6] Y. Peng, S. He, Y. Zhang, Z. Niu, L. Xiao, and T. Jiang, "Ambient LoRa Backscatter System With Chirp Interval Modulation," *IEEE Transactions on Wireless Communications*, vol. 22, no. 2, pp. 1328–1342, 2023.

[7] H. Zhang, G. Liu, Y. Xu, and T. Jiang, "LoRaAid: Underground Joint Communication and Localization System Based on LoRa Technology," *IEEE Transactions on Wireless Communications*, pp. 1–1, 2023.

[8] A. Llap and M. Nunez, "Evaluating Energy Consumption and Maximum Communication Distance for SX1280 LoRa Transceiver at 2.4 GHz towards Adaptive Networks," in *2023 19th International Conference on Wireless and Mobile Computing, Networking and Communications (WiMob)*, 2023, pp. 393–398.

[9] G. H. Derévianckine, A. Guitton, O. Iova, B. Ning, and F. Valois, "Opportunities and Challenges of LoRa 2.4 GHz," *IEEE Communications Magazine*, vol. 61, no. 10, pp. 164–170, 2023.

[10] A. Pagano, D. Croce, I. Tinnirello, and G. Vitale, "A Survey on LoRa for Smart Agriculture: Current Trends and Future Perspectives," *IEEE Internet of Things Journal*, vol. 10, no. 4, pp. 3664–3679, 2023.

[11] P. Kietzmann, J. Alamos, D. Kutscher, T. C. Schmidt, and M. Wählisch, "Rethinking LoRa for the IoT: An InformationCentric Approach," *IEEE Communications Magazine*, vol. 62, no. 1, pp. 34–39, 2024.

[12] Demin Gao,Wenchao Jiang, Weizheng Wang,Zhaoyang Han,Yunhuai Liu, "LoFi: Physical-layer CTC from LoRa to WiFi with IEEE 802.11ax," in *IEEE INFOCOM 2025 - IEEE Conference on Computer Communications*, 2025, pp. 1–10.

[13] X. Ma, P. Zhang, Y. Liu, C. A. Boano, H.-S. Kim, J. Wei, and J. Huang, "Harmony: Saving Concurrent Transmissions from Harsh RF Interference," in *IEEE INFOCOM 2020 - IEEE Conference on Computer Communications*, 2020, pp. 1024–1033.

[14] J. Yao, J. Su, R. Xie, K. Wu, and V. C. M. Leung, "Empowering Heterogeneous Wireless Networks through Efficient Signal Identification," *IEEE Wireless Communications*, pp. 1–7, 2024.

[15] B. Shilpa, P. R. Kumar and R. Kumar Jha, "Spreading Factor Optimization for Interference Mitigation in Dense Indoor LoRa Networks," 2023 IEEE IAS Global Conference on Emerging Technologies (GlobConET), London, United Kingdom, 2023, pp. 1-5, doi: 10.1109/GlobConET56651.2023.10149925.

[16] G. Zhu, C. -H. Liao, M. Suzuki, Y. Narusue and H. Morikawa, "Evaluation of LoRa receiver performance under co-technology interference," 2018 15th IEEE Annual Consumer Communications & Networking Conference (CCNC), Las Vegas, NV, USA, 2018, pp. 1-7, doi: 10.1109/CCNC.2018.8319183.

[17] B. Shilpa, Hari Prabhat Gupta, Rajesh Kumar Jha, and Syed Shakeel Hashmi. "LoRa interference issues and solution approaches in dense IoT networks: a review. Telecommun". Syst. 87, 2 (Oct 2024), 517–539. https://doi.org/10.1007/s11235-024-01192-9

[18] A. Osorio, M. Calle, J. D. Soto, and J. E. Candelo-Becerra, "Routing in LoRaWAN: Overview and Challenges," *IEEE Communications Magazine*, vol. 58, no. 6, pp. 72–76, 2020.

[19] K. Lin, M. A. Ullah, H. Alves, K. Mikhaylov, and T. Hao, "Subterranean mMTC in Remote Areas: Underground-to-Satellite Connectivity Approach," *IEEE Communications Magazine*, vol. 61, no. 5, pp. 136–142, 2023.

[20] D.Gao, L.Ou, Y.Chen, X.Guo, R.Liu, Y.Liu and T.He, "Physical-layer CTC from BLE to Wi-Fi with IEEE 802.11ax," *IEEE Transactions on Mobile Computing*, 2024.DOI:10.1109/TMC.2024.3462941

[21] P. Tian, X. Ma, C. A. Boano, Y. Liu, F. Yang, X. Tian, D. Li, and J. Wei, "ChirpBox: An Infrastructure-Less LoRa Testbed," in *Proceedings of the 2021 International Conference on Embedded Wireless Systems and Networks*, ser. EWSN '21. USA: Junction Publishing, 2021, p. 115–126.

[22] P. Tian, F. Yang, X. Ma, C. A. Boano, X. Tian, Y. Liu, and J. Wei, "Environmental Impact on the Long-Term Connectivity and Link Quality of an Outdoor LoRa Network," in *Proceedings of the 19th ACM Conference on Embedded Networked Sensor Systems*, ser. SenSys '21. New York, NY, USA: Association for Computing Machinery, 2021, p. 565–568.

[23] A. Valkanis, G. A. Beletsioti, K. F. Kantelis, P. Nicopolitidis, and G. I. Papadimitriou, "Ensuring Reliability for LoRa Networks Using a Reinforcement-Learning-Assisted Time Division Duplex Protocol," *IEEE Internet of Things Journal*, vol. 11, no. 3, pp. 4179–4190, 2024.

[24] H. H. R. Sherazi, L. A. Grieco, M. A. Imran, and G. Boggia, "Energy-Efficient LoRaWAN for Industry 4.0 Applications," *IEEE Transactions on Industrial Informatics*, vol. 17, no. 2, pp. 891–902, 2021.

[25] G. Cuozzo, C. Buratti, and R. Verdone, "A 2.4-GHz LoRa-Based Protocol for Communication and Energy Harvesting on Industry Machines," *IEEE Internet of Things Journal*, vol. 9, no. 10, pp. 7853–7865, 2022.

[26] A. Soto-Vergel, L. Arismendy, R. Bornacelli-Durán, C. Cardenas, B. Montero-Arévalo, E. Rivera, M. Calle, and J. E. Candelo-Becerra, "LoRa Performance in Industrial Environments: Analysis of Different ADR Algorithms," *IEEE Transactions on Industrial Informatics*, vol. 19, no. 10, pp. 10 501–10 511, 2023.

[27] G. Anand, M. Vyas, R. N. Yadav, and S. K. Nayak, "On Reducing Data Transmissions in Fog-Enabled LoRa-Based Smart Agriculture," *IEEE Internet of Things Journal*, vol. 11, no. 5, pp. 8894–8905, 2024.

[28] A. Caruso, S. Chessa, S. Escolar, J. Barba, and J. C. López, "Collection of Data With Drones in Precision Agriculture: Analytical Model and LoRa Case Study," *IEEE Internet of Things Journal*, vol. 8, no. 22, pp. 16 692–16 704, 2021.

[29] C. F. Hernández, G. Hochet Derévianckine, A. Guitton, O. Iova, and F. Valois, "Indoor Performance Evaluation of LoRa® 2.4 GHz," in *2023 IEEE Wireless Communications and Networking Conference (WCNC)*, 2023, pp. 1–6.

[30] F. Yang, P. Tian, X. Ma, C. A. Boano, Y. Liu, and J. Wei, "EMU: Increasing the Performance and Applicability of LoRa through Chirp Emulation, Snipping, and Multiplexing," in *2022 21st ACM/IEEE International Conference on Information Processing in Sensor Networks (IPSN)*, 2022, pp. 363–376.

[31] W. Xiao, M. Kaneko, N. El Rachkidy, and A. Guitton, "Integrating LoRa Collision Decoding and MAC Protocols for Enabling IoT Massive Connectivity," *IEEE Internet of Things Magazine*, vol. 5, no. 3, pp. 166–173, 2022.

[32] Q. Chen and J. Wang, "AlignTrack: Push the SNR Limit of LoRa Collision Decoding," *IEEE/ACM Transactions on Networking*, vol. 31, no. 5, pp. 2070–2085, 2023.

[33] S. Tong, Z. Shen, Y. Liu, and J. Wang, "Combating Link Dynamics for Reliable LoRa Connection in Urban Settings," in *Proceedings of the 27th Annual International Conference on Mobile Computing and Networking*, ser. MobiCom '21. New York, NY, USA: Association for Computing Machinery, 2021, p. 642–655.

[34] S. Hong, F. Yao, F. Zhang, Y. Ding, and S.-H. Yang, "Reinforcement Learning Approach for SF Allocation in LoRa Network," *IEEE Internet of Things Journal*, vol. 10, no. 20, pp. 18 259–18 272, 2023.

[35] F. Van den Abeele, J. Haxhibeqiri, I. Moerman, and J. Hoebeke, "Scalability Analysis of Large-Scale LoRaWAN Networks in NS-3," *IEEE Internet of Things Journal*, vol. 4, no. 6, pp. 2186–2198, 2017.

[36] D. Saluja, R. Singh, L. K. Baghel, and S. Kumar, "Scalability Analysis of LoRa Network for SNR-Based SF Allocation Scheme," *IEEE Transactions on Industrial Informatics*, vol. 17, no. 10, pp. 6709–6719, 2021.

[37] D. Saluja, R. Singh, S. Gautam, and S. Kumar, "EWS: Exponential Windowing Scheme to Improve LoRa Scalability," *IEEE Transactions on Industrial Informatics*, vol. 18, no. 1, pp. 252–265, 2022.

[38] A. Petroni and M. Biagi, "Interference Mitigation and Decoding Through Gateway Diversity in LoRaWAN," *IEEE Transactions on Wireless Communications*, vol. 21, no. 11, pp. 9068–9081, 2022.

[39] D.Gao, H.Wang, S.Wang, W.Wang, Z.Yin, M.Shahid, X.Li, F.Valerio and N.Arumugam , "WiLo: Long-Range Cross-Technology Communication from Wi-Fi to LoRa," *IEEE Transactions on Communications*, 2024.DOI:10.1109/TCOMM.2024.3461574

[40] Demin Gao, Haoyu Wang, YongRui Chen, Qiaolin Ye, Weizheng Wang, Xiuzhen Guo, Shuai Wang, Yunhuai Liu, and Tian He, "LoBee: Bidirectional Communication between LoRa and ZigBee based on Physical-Layer CTC," in *IEEE Transactions on Wireless Communications*, 2025, DOI:10.1109/TWC.2025.3556552.

[41] L. Polak, F. Paul, M. Simka, R. Zedka, J. Kufa, and R. Sotner, "On the Interference between LoRa and Bluetooth in the 2.4 GHz Unlicensed Band," in *2022 32nd International Conference Radioelektronika (RADIOELEKTRONIKA)*, 2022, pp. 1–4.

[42] C. Orfanidis, L. M. Feeney, M. Jacobsson, and P. Gunningberg, "Investigating Interference between LoRa and IEEE 802.15.4g Networks," in *2017 IEEE 13th International Conference on Wireless and Mobile Computing, Networking and Communications (WiMob)*, 2017, pp. 1–8.

[43] A. Mukhopadhyay, A. S. Thomas, and R. R. Hegde, "Interference in Large Scale wireless networks: A Case Study with LoRa (Long Range WiFi) and LTE (Long Term Evolution)," in *2019 International Conference on Communication and Electronics Systems (ICCES)*, 2019, pp. 1352–1357.

[44] G. Pasolini, "On the LoRa Chirp Spread Spectrum Modulation: Signal Properties and Their Impact on Transmitter and Receiver Architectures," *IEEE Transactions on Wireless Communications*, vol. 21, no. 1, pp. 357–369, 2022.

[45] Y. He, X. Guo, X. Zheng, Z. Yu, J. Zhang, H. Jiang, X. Na, and J. Zhang, "Cross-Technology Communication for the Internet of Things: A Survey," *ACM Comput. Surv.*, vol. 55, no. 5, dec 2022.

[46] M. J. Faber, K. M. van der Zwaag, W. G. V. dos Santos, H. R. d. O. Rocha, M. E. V. Segatto, and J. A. L. Silva, "A Theoretical and Experimental Evaluation on the Performance of LoRa Technology," *IEEE Sensors Journal*, vol. 20, no. 16, pp. 9480–9489, 2020.

Demin Gao received the Ph.D. degree from the Department of Computer Science and Engineering, Nanjing University of Science and Technology, Nanjing, China, in 2012. From 2011 to 2012, he was a joint Ph.D. student and attended the research lab of Kwan-Wu Chin with the School of Electrical, Computer, and Telecommunications Engineering, University of Wollongong, Wollongong, NSW, Australia. He joined with the College of Information Science and Technology, Nanjing Forestry University, Nanjing, as a Lecturer and an Associate Professor in 2012 and 2016. From 2013 to 2016, he pursued an Advanced Postdoctoral Engineering Training with the School of Computer Science and Engineering, Southeast University, Nanjing. From 2016 to 2017, he was a Visiting Scholar and attended the research lab of Tian He with the Department of Computer Science and Engineering, University of Minnesota Twin Cities, Minneapolis, MN, USA. His current research fields contain routing protocols base on cross-technology communication for delay tolerant, data aggregation and multiconstrained routing algorithms in wireless sensor networks, and energy-harvesting wireless sensor networks.

Ye Liu received the M.S. and Ph.D. degrees in electronic science and engineering from Southeast University, Nanjing, China, in 2013 and 2018, respectively.,From 2014 to 2015, he was a Visiting Scholar with Montana State University, Bozeman, MT, USA. From 2017 to 2018, he was a joint Ph.D. Student with the Networked Embedded Systems Group, RISE Swedish Institute of Computer Science, Kista, Sweden. He is currently a Lecturer with Nanjing Agricultural University, Nanjing. He has authored or coauthored papers in several prestigious journals, such as the IEEE Communications Magazine, IEEE Wireless Communications, IEEE Internet of Things Journal, ACM Transactions on Embedded Computing System, and IEEE Network. His current research interests include the Internet of Things, energy harvesting, and tiny machine learning. Dr. Liu was the recipient of the 1st place of the EWSN Dependability Competition in 2019.

Qiaolin Ye received the Ph.D. degree in pattern recognition and intelligence system from the Nanjing University of Science and Technology, Nanjing, China, in 2013. He is a Full Professor with the Computer Science Department, Nanjing Forestry University, Nanjing, China. He has authored more than 50 scientific articles. His research interests include machine learning, data mining, and pattern recognition. Some of them are published in the IEEE TNNLS, IEEE TIFS, and IEEE TCSVT.

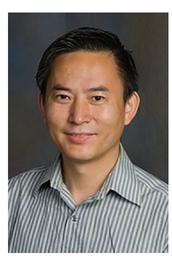

Honggang Wang is the founding Chair and Professor of the Department of Graduate Computer Science and Engineering, Katz School of Science and Health, Yeshiva University in New York City. He was a Professor at UMass Dartmouth (UMassD). He is an alumnus of NAE Frontiers of Engineering program. He graduated 30 MS/Ph.D. students and produced high-quality publications in prestigious journals and conferences in his research areas, winning several prestigious best paper awards. His research interests include Internet of Things and its applications in health and transportation (e.g., autonomous vehicles) domains, Machine Learning and Big Data, Multimedia and Cyber Security, Smart and Connected Health, Wireless Networks, and Multimedia Communications. He is an IEEE distinguished lecturer and a Fellow of AAIA. He has served as the Editor in Chief (EiC) for IEEE Internet of Things Journal during 2020?2022. He was the past Chair (2018-2020) of IEEE Multimedia Communications Technical Committee and the past IEEE eHealth Technical Committee Chair (2020-2021).